

A long-lived band of plasma density enhancement at mid-latitudes during the 2003 Halloween magnetic storm

Jaeheung Park^{a,*}, Hermann Lühr^a, Norbert Jakowski^b, Tatjana Gerzen^b, Hyosub Kil^c, Geonhwa Jee^d, Chao Xiong^{a,e}, Kyoung Wook Min^f, Max Noja^a

^a Helmholtz Center Potsdam (GFZ), German Research Center for Geosciences, Telegrafenberg, D-14473 Potsdam, Germany

^b German Aerospace Center, Institute of Communications and Navigation, Kalkhorstweg 53, D-17235 Neustrelitz, Germany

^c Johns Hopkins University Applied Physics Laboratory, Laurel, MD, USA

^d Division of Polar Climate Research, Korea Polar Research Institute, Incheon 406-840, South Korea

^e Department of Space Physics, College of Electronic Information, Wuhan University, Wuhan 430079, PR China

^f Department of Physics, Korea Advanced Institute of Science and Technology (KAIST), 373-1 Kuseong-dong, Yuseong-gu, Daejeon 305-701, South Korea

ARTICLE INFO

Article history:

Received 29 June 2011

Received in revised form

23 January 2012

Accepted 20 March 2012

Available online 29 March 2012

Keywords:

Storm-enhanced density

Storm-time ionosphere

Ionospheric irregularities

ABSTRACT

During the magnetic storm recovery phase between 08 and 13 UT on 30th October 2003 (so-called Halloween Storm), CHAMP, GRACE and TIMED satellites encountered an unusual post-midnight streak of high plasma density. The streak was latitudinally narrow ($\sim 0.5^\circ$ GLAT), zonally elongated ($> 10^\circ$ GLON), and vertically extended for several hundred kilometers. Inside the streak, as observed by CHAMP, the deviation of the magnetic field from the background is greater in the zonal component than in the meridional component. This observation is consistent with the zonally extended nature of the streak, as confirmed by TIMED/GUVI optical observations. The field-aligned current (FAC) direction is generally upward (downward) at the equatorward (poleward) edge of the streak. We discuss the time history of observed features. We suggest the following scenario of the streak formation. A storm-enhanced density (SED) was generated before 19 h local time by a sub-auroral polarization stream (SAPS). The SED gradually separated from the poleward-retreating region of strong westward plasma drift and turned into an electron density enhancement fossil (EDEF). This EDEF at mid-latitude (about 40° S MLAT) practically co-rotated with the Earth for more than 10 h through the night till dawn. We suggest that the enhanced plasma pressure was counter-balanced by magnetic pressure gradient and kept stable over many hours.

© 2012 Elsevier Ltd. All rights reserved.

1. Introduction

Geomagnetic storms significantly impact the low- and middle-latitude ionosphere (e.g. Greenspan et al., 1991; Jakowski et al., 1991; Lee et al., 2002; Tsurutani et al., 2004, just to name a few), although those regions are not expected to respond directly to changes in the solar wind and magnetosphere. Penetrating E-field, modified wind circulation and/or neutral composition change are the primary drivers of the storm-time ionospheric variations at low and middle latitudes (e.g. Jakowski et al., 2002). One of the spectacular storm-time phenomena is the storm-enhanced density (SED). The SED phenomenon is a sunward-drifting band of enhanced plasma density extending from duskside sub-auroral latitudes to the noontime cusp (Foster and Rideout, 2007, and references therein). SED was first identified over Northern America.

Yizengaw et al. (2006, 2008) reported that such events can also occur in other longitude sectors. A SED event is magnetically conjugate to the drainage plume at plasmaspheric altitudes (Foster et al., 2002). Foster and Rideout (2007) showed that SED plumes appear hemispherically conjugate in general.

Sub-Auroral Polarization Stream (SAPS) is a high-speed westward (sunward at dusk) flow of sub-auroral plasma (e.g. Foster and Vo, 2002; Wang et al., 2011a). The equatorward edge of SAPS is collocated with a SED event (Foster et al., 2007). The dayside and pre-midnight mid-latitude plasma density is enhanced by the storm-induced penetration of the zonal/meridional electric field (Vlasov et al., 2003; Kelley et al., 2004), and the sunward/poleward transport of the high-density plasma by SAPS creates the elongated SED at the SAPS equatorward edge (Foster et al., 2007). A SED does not co-rotate, but it is transported sunward by a SAPS (Foster et al., 2004). After reaching the cusp it can turn into a tongue-of-ionization (TOI) at the dayside cusp (e.g. Foster and Rideout, 2007, and references therein). Because the latitudinal width, average speed, and occurrence rate of SAPS events are largest before

* Corresponding author. Tel.: +49 331 288 1955.

E-mail address: park@gfz-potsdam.de (J. Park).

midnight (see Figures 4, 5, and 8 of Foster and Vo, 2002, and references therein) and since the resultant SED convects sunward, it might be natural to expect less SED events after midnight. Actually, most of the SED events reported previously occurred during daytime and in the pre-midnight sector (e.g. Foster, 1993; Foster et al., 2002; Yizengaw et al., 2005, 2006; Foster and Rideout, 2007; Pokhotelov et al., 2008). To our knowledge there has been no dedicated study on a post-midnight SED event.

We report an unusual post-midnight streak of high plasma density, which is presumed to originate from a SED, observed during the 30th October 2003 magnetic storm. This storm is known as the Halloween storm. Multiple instruments (plasma, neutral, magnetic, radio wave and optical) onboard the Challenging Mini-Satellite Payload (CHAMP) and the Thermosphere Ionosphere Mesosphere Energetics and Dynamics (TIMED) spacecraft are used to clarify the 3D structure of the streak. Defense Meteorological Satellite Program (DMSP), the Ocean Topography Experiment (TOPEX), and Gravity Recovery And Climate Experiment (GRACE) satellites are used to track the evolution of the streak. In the next section we briefly describe the instruments and the background geophysical conditions around the Halloween storm. The observations are given in Section 3, and discussed in detail in Section 4. Section 5 summarizes the results and draws conclusions. Note that there are a variety of storm-time TEC enhancements (positive ionospheric storm) at different latitudes, for which the term, ‘SED’ has been ambiguously used at times (see Section 1.1 of Foster et al., 2007). In this study, however, the term ‘SED’ is exclusively used to designate the pre-midnight thin plume of storm-time plasma density enhancement stemming from the large-scale reservoir (so-called ‘bulge’ in Datta-Barua et al., 2011) at lower latitudes. For similar plumes in the ‘post-midnight’ sector we use the term electron density enhancement fossil (EDEF).

2. Instruments and background conditions

The altitude of CHAMP was about 450 km at launch in 2000, and decayed to about 400 km on 30th October 2003. The satellite circled the Earth on a polar (inclination angle=87°) orbit. CHAMP carried an accelerometer measuring neutral mass density and zonal wind every 10 s, a Planar Langmuir Probe (PLP) measuring electron density and temperature every 15 s, a Flux-Gate Magnetometer (FGM) providing the magnetic field vector at a 50 Hz rate, and a Digital Ion Drift Meter (DIDM) measuring plasma density and drift velocity every second. Unfortunately, DIDM was severely degraded during the launch and can provide only uncalibrated plasma density. The resolution of the neutral mass density is better than 1×10^{-14} kg/m⁻³ (Liu et al., 2005). Precision of zonal wind velocity amounts to 20 m/s (Liu et al., 2006), and that of plasma density as observed by the PLP is 4% with a spread of about 10% (McNamara et al., 2007; Liu et al., 2007). Electron temperature as observed by the PLP is about 3% lower than radar observations with a standard deviation of 8% (Rother et al., 2010). A flux-gate magnetometer delivers vector field readings at a rate of 50 Hz and with a resolution of 0.1 nT (Lühr et al., 2004; Stolle et al., 2006).

While the above-mentioned instruments measure ionospheric and thermospheric parameters at the position of the satellite, the Global Positioning System (GPS) receiver onboard CHAMP can estimate topside total electron content (TEC) between CHAMP and GPS satellites. The TEC data can be used for a 2D (altitude-latitude) reconstruction of the ionospheric density. To generate the electron density profiles, TEC values calculated from the CHAMP-GPS measurements are assimilated into the Parameterized Ionospheric Model (PIM) (Heise et al., 2002).

The TIMED satellite is at an altitude of 630 km, and the inclination angle of the orbit is 74°. The Global Ultraviolet Imager (GUVI) onboard TIMED scans airglow intensity below the satellite with a scanning mirror to construct 2D (longitude-latitude) images at five different wave lengths. Among them is the 135.6 nm nightglow, whose intensity is approximately proportional to the vertical total electron content (TEC) (Kil et al., 2004). It will be used in this paper.

DMSP F13, F15, and F16 are on circular (altitude ~ 840 km) and sun-synchronous orbits. The local time (LT) of the F13/15/16 orbit is 0600-1800/0930-2130/0810-2010 h, respectively. The Special Sensors-Ions, Electrons, and Scintillation (SSIES) onboard the satellites measure ion/electron density/temperature, plasma drift vector, and ion composition at the satellite positions. The data of F13 and F15 are open to public at <http://cindispace.utdallas.edu/DMSP/index.html>. Keyser et al. (2003) reported that plasma densities, as observed by the DMSP/SSIES, are typically lower than radar observations, but this will not significantly compromise the current study because we are mainly interested in the variation of plasma density. According to Drayton et al. (2005) the cross-track plasma drift velocity shows good correlation with ground-based radar observations (correlation coefficient=0.9), but the magnitude is slightly larger than the radar observations (by a factor of 1.4).

The TOPEX satellite is at an altitude of 1330 km, and the orbit inclination angle is 66°. The satellite observes TEC between the sea surface and its orbital altitude. GRACE consists of two satellites cruising at polar (inclination angle=89°) circular (about 500 km) orbits. Using data from its K-band ranging system we can estimate the average plasma density between the dual satellites (inter-satellite separation ~ 220 km) (Xiong et al., 2010). The estimated plasma density may have a bias level uncertainty (Lühr and Xiong, 2010), but it has little effect on the current study because we focus on the variation of plasma density as observed by GRACE. The GPS receiver onboard GRACE can estimate topside TEC between GRACE and GPS satellites.

Fig. 1 shows the evolution of the auroral activity (AE) and storm-time D_{ST} indices during the Halloween storm (data available

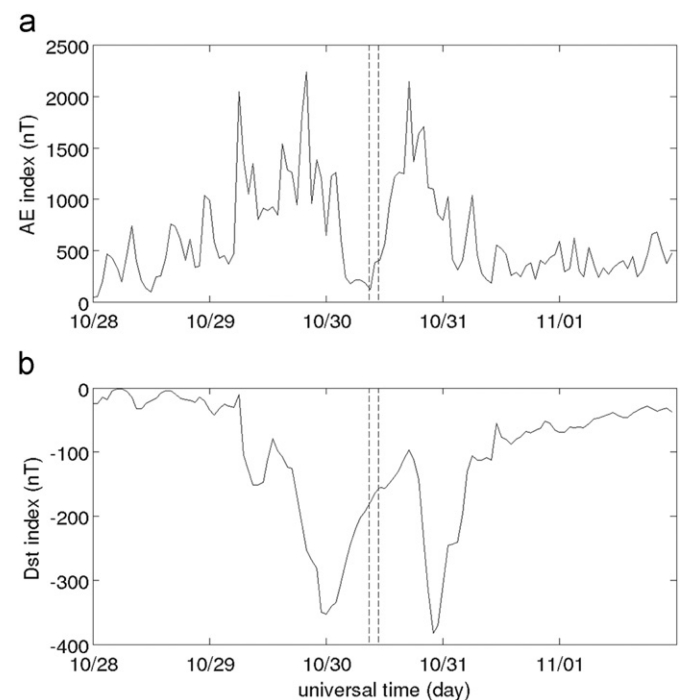


Fig. 1. Evolution of AE and D_{ST} indices during the Halloween storm. The time interval of prime interest (from 08:44 UT to 10:46 UT on 30th October 2003) is marked by dashed lines.

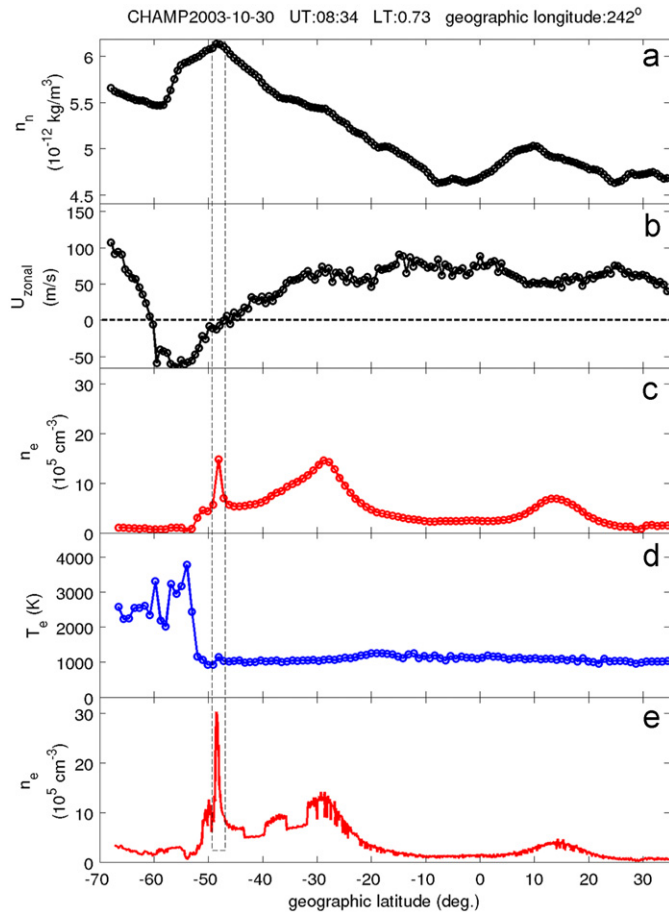


Fig. 2. CHAMP observations around 08:46 UT on 30th October 2003: (a) neutral density, (b) zonal neutral wind (positive eastward), (c and d) electron density/temperature measured by PLP, and (e) electron density measured by DIDM and scaled to PLP data.

at <http://omniweb.gsfc.nasa.gov/>). There were three consecutive storms in total during the Halloween events. The first and second storm began on 29th October, and the second storm attained its D_{ST} minimum near 00 UT on 30th October 2003. Around 08:44 UT on 30th October 2003 (marked by dashed lines in Fig. 1) CHAMP passed the nightside at 01 LT (post-midnight). It was right in the middle of the recovery phase of the second storm, separated from the previous (following) storm main phase by about 8 (9) h. In this paper we investigate the ionospheric evolution between 00–14 UT, but focus on the time period from 08:44 UT to 10:46 UT on 30th October 2003.

3. Observation

Fig. 2 shows from top to bottom (a) neutral density, (b) zonal wind (positive eastward), (c and d) electron density/temperature measured by PLP, and (e) electron density measured by DIDM (scaled to PLP data). The magnetic equator for this CHAMP pass was at 5.4°S geographic latitude (GLAT). Near 48°S GLAT and 242°E geographic longitude (GLON) CHAMP observed a narrow plasma density anomaly (hereafter called EDEF, the use of the term will be justified later by the TIMED/GUVI observation) with the maximum reaching 300% of the ambient density (panel e). The corresponding magnetic latitude (MLAT) is 40°S ($L = 1.82R_e$, apex height: 5200 km). The electron density peak coincides with a broader neutral density maximum, but the wind shows no conspicuous change. Neutral wind was approximately at rest at the location of the plasma density peak within the EDEF. The electron temperature shows a slight enhancement ($< 200\text{ K}$) at the EDEF peak position.

Fig. 3 shows the magnetic signatures of the EDEF as observed by the CHAMP/FGM. The data are presented in Mean-Field-Aligned (MFA) coordinates, which are defined as follows: parallel (along the mean field), zonal (perpendicular and to magnetic east), and meridional (completing the triad, positive outward). The mean field direction at each point is calculated by averaging

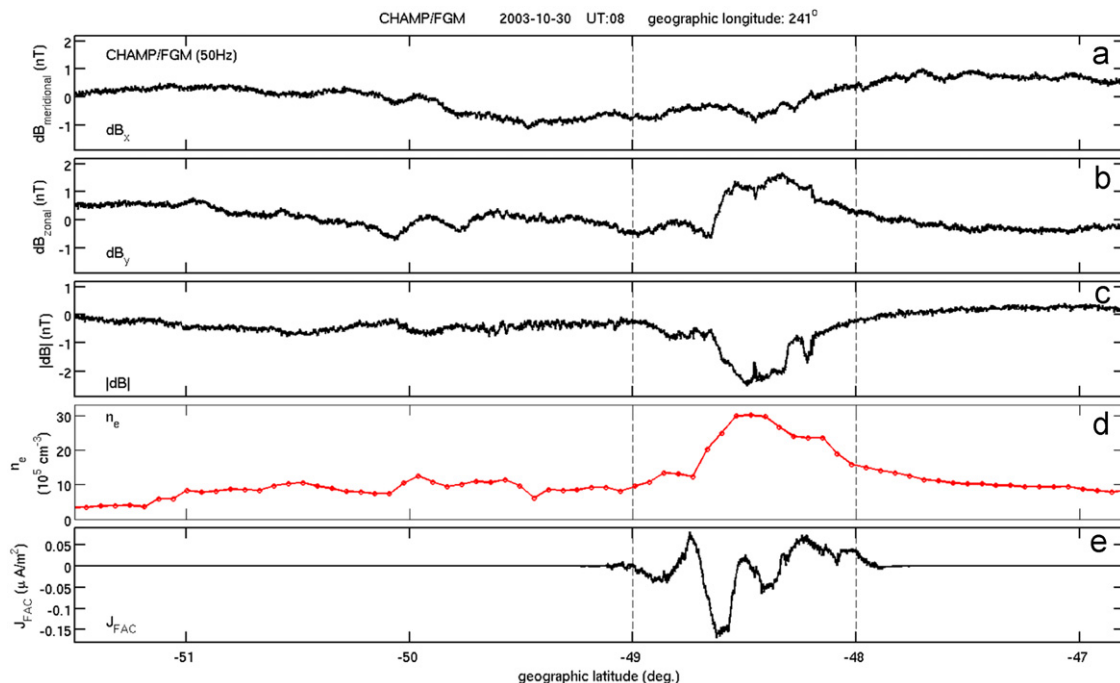


Fig. 3. Magnetic signature of the EDEF as observed by CHAMP/FGM. Panels (a) and (b) present transverse components of the B-field in the meridional and zonal directions, respectively. Panel (c) is residual of magnetic field strength, and panel (d) the plasma density repeated from Fig. 2(e). Panel (e) shows the FAC density (positive upward) around the EDEF. Downward currents are observed at the poleward edge and upward at the more gentle equatorward slope.

observed data with a 201 s-long Savitzky–Golay filter. Panels (a) and (b) present the meridional and zonal components, respectively. Panel (c) represents residual variations of the total magnetic field strength after subtracting the mean field. Panel (d) is the plasma density repeated from Fig. 2(e). Inside the EDEF the B-field strength is reduced (panel c), the zonal B-field component exhibits an anti-correlation with the field strength (panel b). The meridional B-field, on the other hand, varies weakly showing little correlation with the other components. As the transverse deflections of the B-field are primarily confined to the zonal component inside the EDEF, we can reliably estimate the field-aligned current (FAC) density, j , from the along-track gradient of the zonal component

$$j = \frac{1}{\mu_0} \frac{1}{v_{trans}} \frac{dB_{zonal}}{dt} \quad (1)$$

where v_{trans} is the component of CHAMP velocity perpendicular to the magnetic L shell (estimated to be 5 km/s), dt the temporal spacing between adjacent data points, and μ_0 the permeability of free space. Panel (e) shows the FAC density (positive upward, i.e. parallel to the mean field) around the EDEF. We can see that FACs are predominantly downward (upward) around the poleward (equatorward) edge. Note that the FACs in Fig. 3e are latitudinally well separated from the auroral FAC circuits, which started beyond 47°S MLAT as observed by the CHAMP/FGM (e.g. Figure 3 of Wang et al., 2006).

Fig. 4 shows a 135.6 nm airglow image obtained by GUVI onboard the TIMED satellite. TIMED crosses the equator from south to north, and each equatorial pass moves from east to the west by about 26° in GLON. One orbit takes about 100 min. Note that Fig. 4 is not taken at a certain time, but it is a composite image of successive observations. For each pass the time of equator crossing is given on the top. In Fig. 4 we can see a zonally elongated, narrow enhancement of airglow emission around 50°S and 240°E; a white stripe enframed by a blue box. The observation time is near 10:46 UT (about 2.8 LT), i.e. ~2 h later than the CHAMP observations.

The color map in Fig. 5 represents the 2D plasma density reconstruction by assimilating CHAMP/GPS observations into PIM. The thick solid white curve shows the in situ plasma density as observed by CHAMP/PLP. The horizontal white dashed line is the CHAMP orbital altitude. Slant thin lines represent the magnetic field lines. The latitudinally broad (70°S ~ 20°S GLAT) electron density structure below 500 km altitude reflects the F-region peak. We can identify an isolated enhancement of plasma density around 50°S

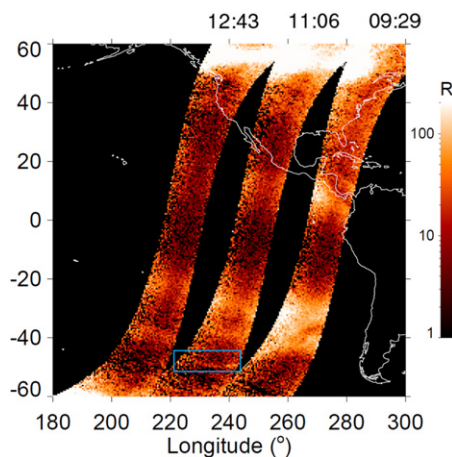


Fig. 4. Airglow images at 135.6 nm obtained by TIMED/GUVI. Time stamps at the top correspond to the equator crossings of the satellite. A zonally elongated enhancement of airglow emission (marked by a rectangle) is observed around 50°S and 240°E near 10:46 UT. (For interpretation of the references to color in this figure legend, the reader is referred to the web version of this article.)

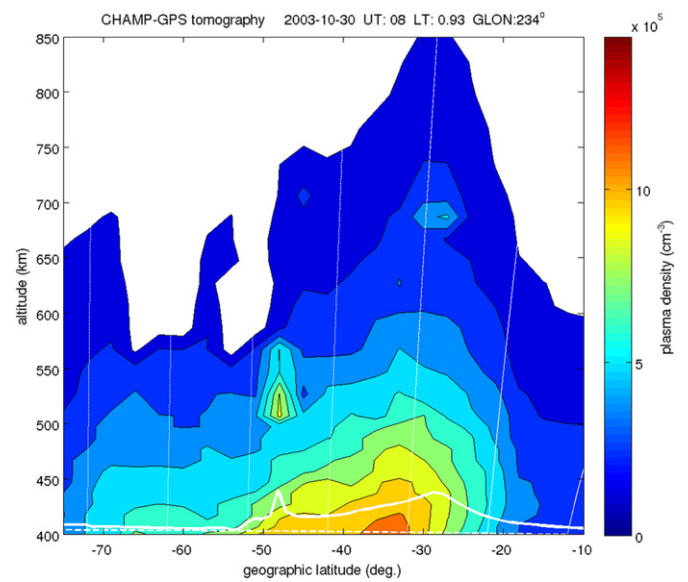


Fig. 5. Meridional cut through ionospheric density. The contours represent the 2D plasma density distribution as derived from CHAMP TEC data assimilation. The white solid line shows the in situ electron density as observed by CHAMP/PLP, and the white dashed horizontal line marks the orbit altitude. The slant thin lines are mean magnetic fields. The magnetic equator is at -5.4° GLAT. (For interpretation of the references to color in this figure legend, the reader is referred to the web version of this article.)

GLAT between 500 km and 550 km altitudes, which seems to be related to the EDEF observed by CHAMP/PLP around 400 km altitude (white solid line). The height resolution of the density reconstruction is 10 km below 500 km altitude and 20–30 km between 500 km and 1000 km altitudes. Considering the limitations of vertical ionospheric profiles reconstructed from GPS/TEC observations (e.g. Wen et al., 2008), we expect that the EDEF is elongated continuously upward between 400 km (CHAMP/PLP data) and 550 km altitudes. The plasma density enhancement between 500 km and 550 km (color map) appears to be latitudinally wider than the EDEF observed by CHAMP/PLP (white solid line). However, the narrow latitudinal width of the EDEF ($< 1^\circ$ GLAT) cannot be estimated precisely by the reconstruction due to the limited resolution (3° GLAT). The overall structure seems nearly field-aligned (tilted slightly equatorward with altitude) and located above the F-region peak.

In order to check the reliability of the plasma density feature at 500 km altitude in Fig. 5, we inspected individual CHAMP slant TEC (STEC) readings that were used to construct the 2D plasma density map. As can be seen in Fig. 6a, there is a narrow STEC peak that coincides with the in situ EDEF detection as shown in Figs. 2 and 3. Similar conspicuous STEC peaks could be deduced from the signals of four more GPS satellites at the same time. This multiple coincidence makes us to believe that the vertical extension of the EDEF (Fig. 5) is real. The GPS satellite 30 (PRN-30) was nearly at zenith for CHAMP (elevation angle $> 80^\circ$) when the STEC between the two satellites exhibited a narrow peak at the EDEF (Fig. 6a). Hence, the vertical TEC (VTEC) gradient can be approximated from the STEC gradient of this observation. The maximum STEC gradient is about 17 TECU/degree. This value is smaller than the record-high value of ‘duskside’ VTEC gradient (50 TECU/degree) shown in Figure 8 by Vo and Foster (2001). Our STEC gradient of about 17 TECU/degree, however, does not reflect the full gradient because (1) we only consider the topside ionosphere above 400 km and (2) the EDEF is expected to be aligned with the magnetic field lines (see Fig. 5). More appropriate is therefore to estimate the TEC gradient transverse to the magnetic L -shells. Taking into account

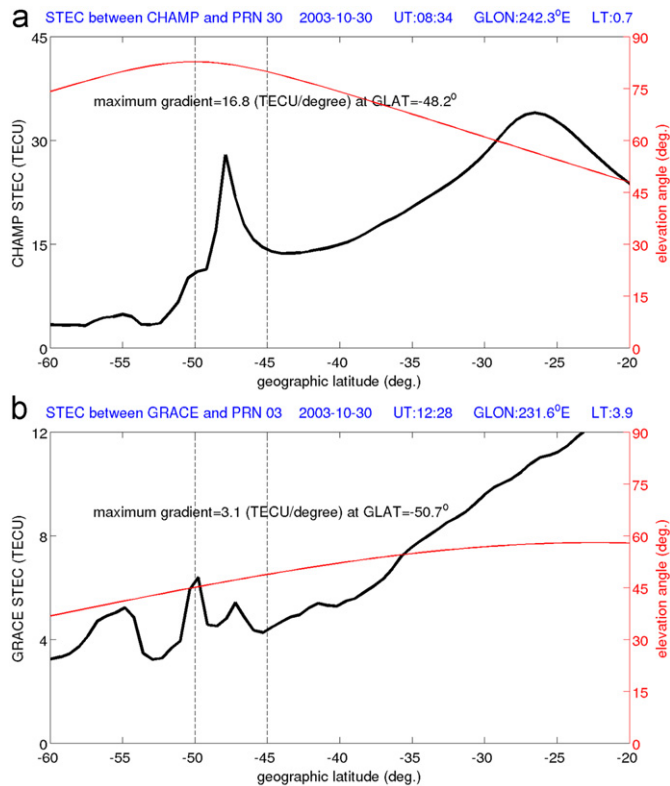


Fig. 6. Latitude profiles of slant TEC as observed by (a) CHAMP and (b) GRACE.

the tripling of the electron density within a sub-degree stripe (see Fig. 3) and background TEC of about 40 TECU (shown later in Fig. 9d), we estimate TEC gradient transverse to the magnetic L -shells to be more than 100 TECU/degree. This is expected to be very harmful to GPS navigation signals.

4. Discussions

4.1. Three-dimensional structure of the EDEF

Here, we discuss the spatial structure of the observed EDEF in more detail. CHAMP/PLP and FGM observed signatures of a latitudinally confined ($\sim 0.5^\circ$ GLAT) EDEF at 08:34 UT (about 0.7 LT). TIMED/GUVI observed 2 h later a thin strip of TEC enhancement (Fig. 4) at a similar GLON and GLAT position (around 02–03 LT sector), although the enhancement is not as conspicuous as in Fig. 2. The strip is azimuthally elongated ($> 10^\circ$ GLON), and its latitudinal extent is very small. Zonal B-field deflections (Fig. 3) originate from FACs along the EDEF walls. Hence, the dominance of the zonal component shown in Fig. 3 is consistent with the shape of the EDEF observed by TIMED/GUVI. It adds credence to the argument that the two satellites observed the same phenomenon. From Fig. 5 we inferred that the overall EDEF structure is nearly field-aligned between 400 km (CHAMP/PLP data) and 550 km (reconstruction data) altitudes. Combining Figs. 2–5 leads us to conclude that the EDEF was (1) latitudinally narrow ($\sim 0.5^\circ$ GLAT), (2) zonally elongated ($> 10^\circ$ GLON), and (3) vertically elongated (probably field-aligned) by several hundreds of kilometers above the F-region peak altitude.

4.2. Possible origins of the EDEF

Let us discuss the origin of the post-midnight EDEF. We can imagine several possibilities to enhance plasma density in the

nightside mid-latitude ionosphere: (1) transport of dense dayside plasma across the polar cap, (2) upward transport of plasma by transverse ion heating (e.g. by waves) and enhanced mirror force, (3) local ionization by soft particle precipitation, or (4) a plasma plume (i.e. SED) generated by SAPS, which drains higher-density plasma from the lower-latitude reservoir. The EDEF occurred at 40° S MLAT (apex height: 5200 km, $L = 1.82R_e$). The location was well separated from the main auroral FAC circuits, which started beyond 47° S MLAT as observed by CHAMP/FGM (see Section 3). Hence, mechanism (1) is rejected because transport of dayside plasma across the polar cap diverges zonally around the equatorward boundary of the nightside auroral oval (Pryse et al., 2006). Likewise, mechanism (2) seems inappropriate to explain our EDEF as they generally occur at the cusp, auroral oval, or polar cap (e.g. Schunk, 2000; Kasahara et al., 2001).

The amplitudes of local FACs around the EDEF were quite small (of the order of $0.1 \mu\text{A}/\text{m}^2$). Directions of the local FAC were on average downward (upward) at the poleward (equatorward) edge; with the downward one showing larger amplitude. Electron temperature shows no large enhancement at the maximum electron density (< 200 K). Compare, for example, our Fig. 2c–e with Figure 1 of Liu et al. (1995). All these observations rule out the possibility that the EDEF might originate from auroral electron precipitations.

Sakaguchi et al. (2007) observed a latitudinally narrow ($< 1^\circ$ GLAT) and zonally elongated proton arc at $L \sim 4$, which was associated with proton precipitation enhancement at 30–80 keV energy range. One may ask whether our EDEF originated from such proton precipitation. We checked the 30–80 keV proton precipitation as observed by the NOAA-POES 16 (17) satellites at the post-(pre-)midnight sector (data not shown here, but available at <http://satdat.ngdc.noaa.gov/sem/poes/data/avg/txt/>). Between 00–12 UT on 30th October, no localized enhancement of proton precipitation was observed in the energy range near $L \sim 1.8$ around local midnight. The DMSP F16 satellite was at 50° S GLAT and 245° E GLON (near the EDEF location as given in Figs. 2 and 4) around 20:43 LT/04:23 UT on 30th October (about 4 h before the CHAMP-EDEF encounter). The satellite observed no strong proton precipitation (data not shown here, but available at <http://sd-www.jhuapl.edu/Aurora/spectrogram/index.html>). Also the 121.6 nm airglow images taken by TIMED/GUVI (data not shown here, but available at <http://guvi.jhuapl.edu>), which reflect proton precipitation (Immel et al., 2002) do not show an outstanding enhancement at the EDEF location. The proton arc shown in Sakaguchi et al. (2007) was conjugate to the plasma trough in the opposite hemisphere, but our EDEF is well equatorward of the plasma trough (see Fig. 2). Note also that the L value of our EDEF is only 1.82, which is much lower than that ($L \sim 4$) of Sakaguchi et al. (2007). Based on all these observations, although they are not at the exact location and time of the EDEF as observed by CHAMP, we state that proton precipitation cannot be a dominant source of the EDEF and reject mechanism (3).

Mechanism (4) attributes the EDEF to SAPS. Let us track the evolutionary history of SAPS and SED in the southern hemispheric pre-midnight sector, using the in situ observations of DMSP F13 (at dusk) and F15 (at pre-midnight sector) at 840 km altitude. Fig. 7 shows the time series (from top to bottom) of plasma density (black line) and cross-track plasma drift velocity (red line: positive is approximately sunward-westward). The left and right columns correspond to DMSP F13 and F15, respectively. Observations at similar GLON by the two DMSP satellites are presented side-by-side in Fig. 7. But, the UT and LT differ by 2.5–3 h. In panels a and b the cross-track plasma drift speed as observed by DMSP F13 is larger than 1500 m/s around 45° S MLAT. From the DMSP data of auroral particle precipitation (not shown here, but available at <http://sd-www.jhuapl.edu/Aurora/spectrogram/index>).

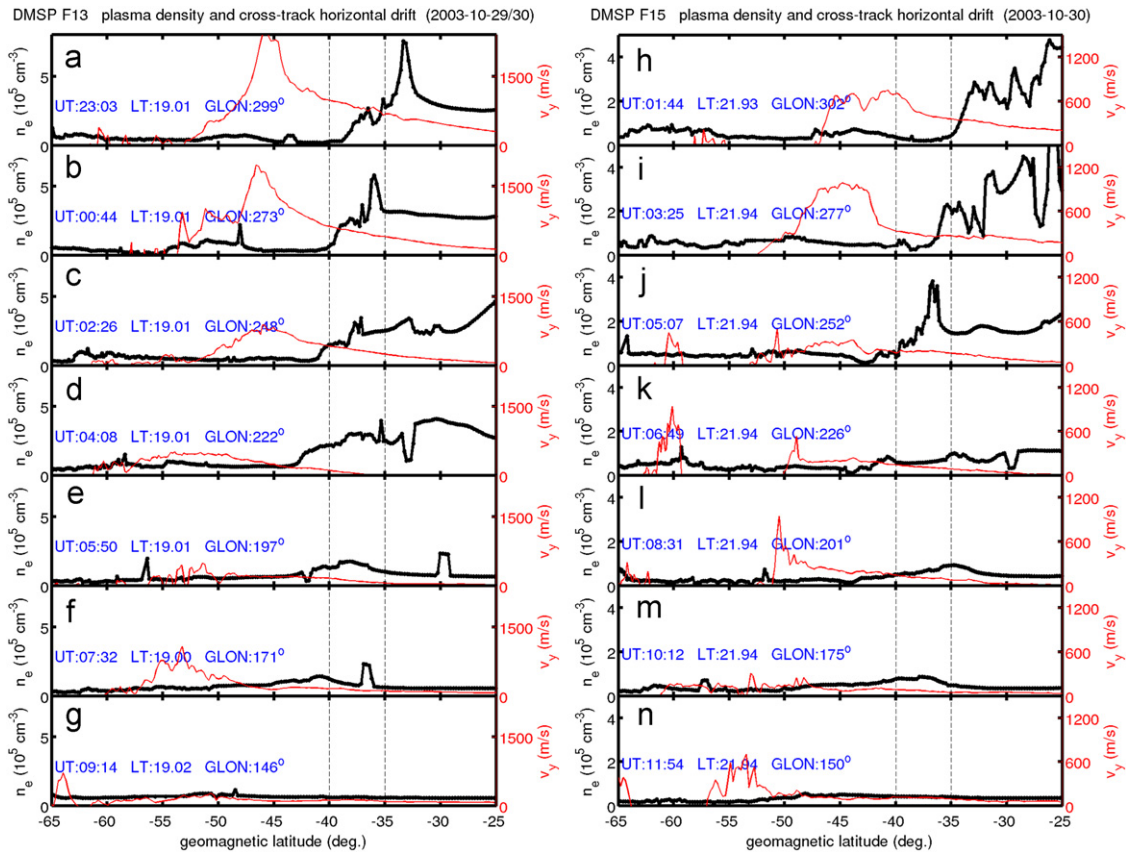


Fig. 7. Time series (from top to bottom) of plasma density and cross-track plasma drift velocity (positive values approximately corresponding to sunward-westward direction) in the southern hemispheric nightside. The left and right columns correspond to DMSF F13 and F15 observations, respectively. Horizontally adjacent panels show observations in a similar GLON sector. (For interpretation of the references to color in this figure legend, the reader is referred to the web version of this article.)

html), the westward drift peaks were located equatorward of the auroral oval. From the latitude (sub-auroral) and westward speed ($> 500 \text{ m/s}$), the region around the westward velocity maximum can be identified as a SAPS (e.g. Wang and Lühr, 2011b). The equatorward part of the SAPS overlaps with the mid-latitude ionospheric plasma enhancement starting at of about 40°S MLAT. There is a narrow density peak between 40°S and 30°S MLAT (latitudinal width $\sim 2^\circ$ GLAT), which migrates poleward from panel a to panel b. The observed density peak can be deemed as a SED based on the generally accepted SED formation mechanism: a SED is formed at the overlap between enhanced westward plasma drift (SAPS) and dense mid-latitude plasma (e.g. Foster et al., 2002). About 3 h after each F13 orbit F15 passed similar GLON sectors. The corresponding F15 data are shown in panels h and i. No evidence of a SED signature was encountered by F15, which implies that the SED in panels a and b did not co-rotate with the Earth. From the SED encounter on successive orbits of F13 at constant LT (panels a and b), it is rather plausible that the SED was nearly sun-synchronous: the westward migration speed of the SED structure is nearly comparable to the eastward rotation speed of the Earth. In the third row both F13 (panel c) and even more clearly F15 (panel j) observed a SED in a similar GLON, while in the fourth row (panels d and k) they barely observed SED-like undulations. This results imply that the SED no longer moves sun-synchronously at that time. Later passes of F13 and F15 (panels e–g and l–n) encountered no conspicuous SED between 40°S and 35°S MLAT (the peak in panel f seems to be an artefact). The fact that the SED was observed in panels c and j implies that it moved towards later LT at about the co-rotation speed without large changes of GLAT and GLON. Hence, Fig. 7 implies that the SED created at 19 LT was nearly sun-synchronous until 02:26 UT

on 30th October 2003, and it migrated towards later LT thereafter. The SED shifting to later LT may have led to the EDEF as observed by CHAMP and TIMED/GUVI past midnight.

Location of the maximum westward speed in Fig. 7 (see the red lines) on average retreated poleward with the peak amplitude weakening accordingly. Simultaneously, cross-track plasma drift speed between 40°S and 35°S MLAT decreased significantly from panel a to panel d (also from panel h to panel k), and remained low afterwards. Note that this cross-track plasma drift was measured at a fixed LT.

Fig. 8 shows a time series of auroral intensity at the nitrogen Lyman–Birge–Hopfield (LBH) band 2 (165–180 nm) as observed by TIMED/GUVI (available at <http://guvi.jhuapl.edu>). The oval-shaped regions of enhanced emission can be regarded as the auroral oval. Each image is drawn on geographic coordinates, and the approximate EDEF position as observed by CHAMP/PLP (50°S , 240°E) is indicated with a cross. Around 00:59 UT (first panel) the auroral oval expanded a lot and came close to 50°S and 240°E . From 02:34 UT (second panel) onward the oval keeps retreating poleward, and the separation from the cross increases. At 10:38 UT (bottom left panel), when TIMED/GUVI observed the band structure in 135.6 nm emission (Fig. 4), the cross was separated from the auroral oval approximately by 20° GLAT. Fig. 8 shows that the auroral oval kept retreating from 00:59 UT to 12:17 UT on 30th October (storm recovery phase). As a SAPS is generally several degrees equatorward of the auroral oval (e.g. Goldstein et al., 2003, and references therein), the SAPS (if it exists) also should retreat poleward following the auroral oval. In other words, the mid-latitude ionosphere at a certain GLAT/GLON becomes more and more free from effects of the high-latitude convection system.

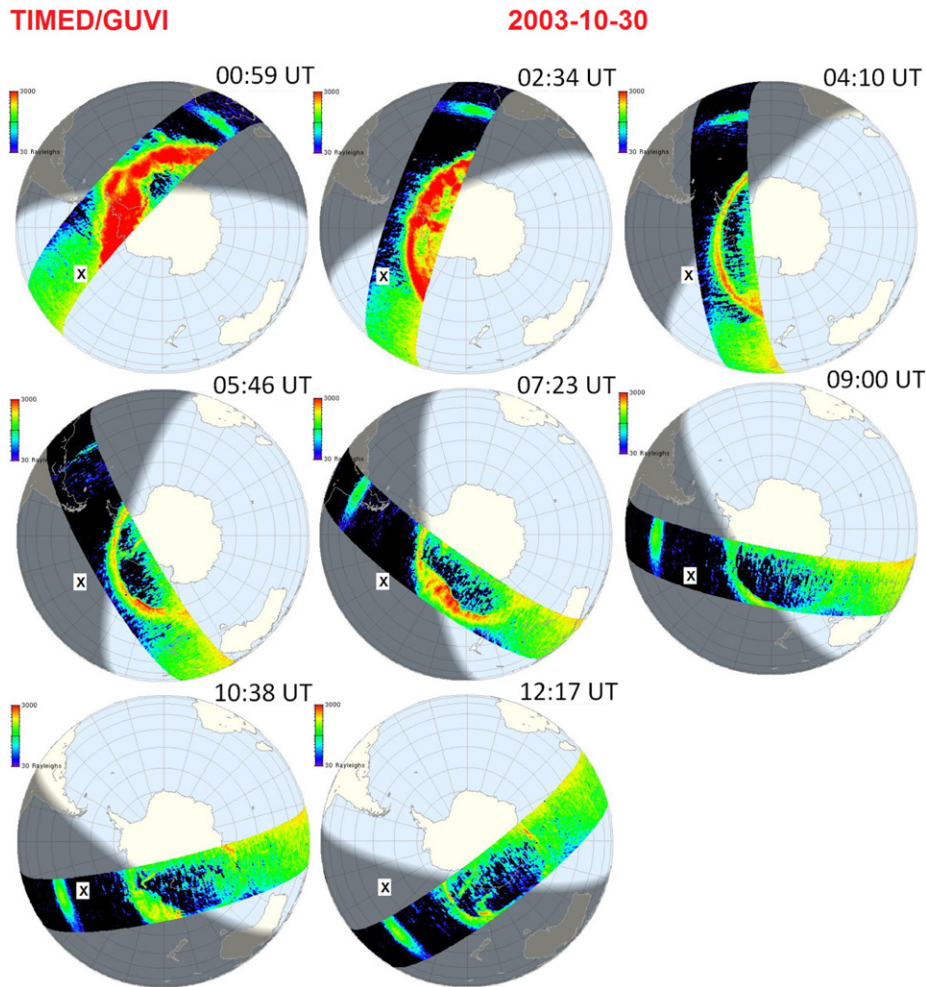


Fig. 8. Time series of auroral intensity at the nitrogen Lyman–Birge–Hopfield (LBH) band 2 (165–180 nm) as observed by TIMED/GUVI. Each image is drawn on geographic coordinates, and the approximate EDEF position as observed by CHAMP/PLP (50°S, 240°E) is indicated with a cross. Given time stamps correspond to the highest magnetic latitude in the southern hemisphere.

Figs. 7 and 8 suggest that westward plasma drift at a certain latitude decreased with UT as the storm went through the recovery phase. Note that drift velocity of the ambient plasma (as given in Fig. 7) doesn't need to be the same in magnitude as migration velocity of SED structure. Nevertheless, the decreasing trend of ambient plasma velocity with UT, as suggested by Figs. 7 and 8, is compatible with our suggestion that westward drift of the SED structure reduced significantly with UT.

4.3. Temporal evolution of the EDEF

In the previous subsection the pre-midnight observations of DMSP and TIMED/GUVI imply possible connection of the pre-midnight SED (as observed by DMSP satellites) to the post-midnight EDEF (as observed by CHAMP and TIMED/GUVI). Near the time of the SED and EDEF event the TOPEX satellite observed TEC between the sea surface and 1330 km altitude in the pre-midnight sector. The GRACE satellites observed plasma density and TEC in the post-midnight sector. We use these observations in combination with the DMSP observations to track the evolutionary history of the EDEF. Fig. 9a–h shows plasma density or TEC (thick lines) and cross-track plasma drift (thin lines) from satellite passes between 220°E and 280°E GLON. The time stamp of each panel corresponds to the satellite crossing of 45°S GLAT, and the UT increases from panel a to h. The region of interest, i.e. between 45° and 50°S GLAT, is bounded by thin dashed grid

lines in each panel in the left column. In Fig. 9i satellite tracks are overlotted onto GUVI 135.6 nm airglow image with the same color and line style as in Fig. 9a–h. Note that there is one exception for the color matching – DMSP F15; the satellite tracks are drawn in white (right column). Enhancements of plasma density or TEC are marked on the satellite tracks by larger solid circles. The satellite tracks in Fig. 9i are projected vertically down onto the airglow layer (not projected along the magnetic field lines). The yellow dashed curves in Fig. 9i represent contours of constant MLAT.

Around 00:44 UT/19.0 LT/273°E GLON (Fig. 9a) the cross-track plasma drift speed peaked near 60°S GLAT, and at a large drift speed of about 2000 m/s; it is the signature of a SAPS as discussed above. There is a small density enhancement, deemed as a SED, around 49°S GLAT (latitudinal width $\sim 2^\circ$ GLAT). The cross-track (nearly westward) speed at this latitude is about 430 m/s. A strong westward drift at the SED location implies that the SED was under active development when it was observed by DMSP F13. Around 02:26 UT/19.0 LT/246°E GLON (Fig. 9b) the cross-track plasma drift speed peaked near 57°S GLAT, and had reduced to about 900 m/s. The equatorward part of this SAPS still overlaps with the mid-latitude ionospheric plasma enhancement at 50°S GLAT and below. The small density peak around 47°S GLAT is regarded as the SED that is at the center of this study.

Due to the large time difference between the DMSP F13 and TIMED/GUVI observations (about 7 h), it may be questionable to relate the two satellite observations to the same phenomenon.

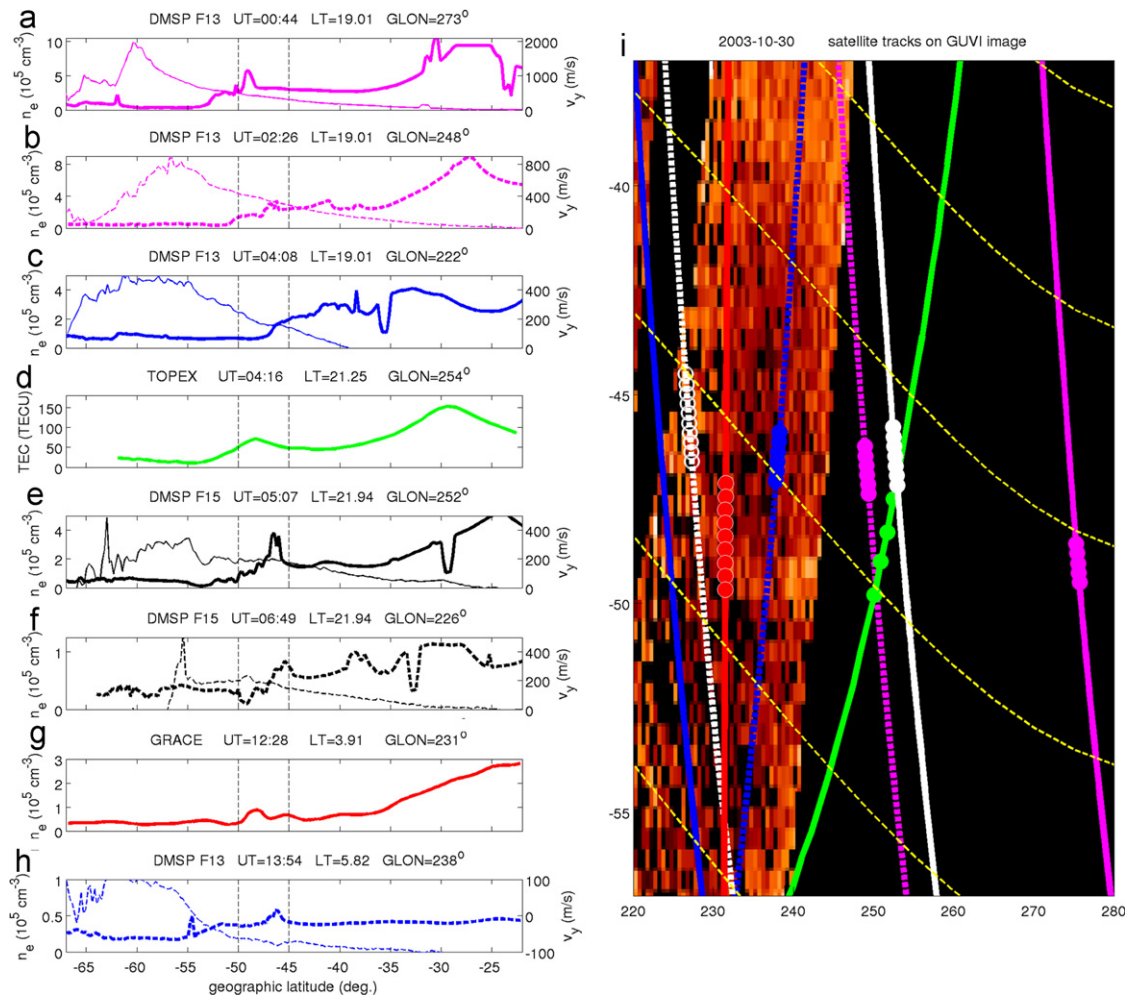


Fig. 9. The left column (panels a–h) shows plasma density/TEC (thick lines) and cross-track plasma drift (thin lines) of DMSP F13, TOPEX, DMSP F15, and GRACE satellites. In the right column (panel i) satellite tracks (thick lines) are overplotted onto the GUVI 135.6 nm airglow image with the same color and line style (solid or dashed) as in panels a–h. Note that there is one exception for the color matching – DMSP F15; the satellite tracks are drawn in white (right column). The region of interest, i.e. between 45° and 50° S GLAT, is bounded by thin dashed grid lines in each panel in the left column. Enhancements of plasma density or TEC are marked on the satellite tracks by larger circles. The yellow dashed curves represent contours of constant MLAT. (For interpretation of the references to color in this figure legend, the reader is referred to the web version of this article.)

Nevertheless, it is interesting to note that the SED observed by DMSP F13 around 02:26 UT/19.0 LT appears at a location (47°S GLAT/248°E GLON) eastward/equatorward of the narrow bright stripe in the TIMED/GUVI image (see Fig. 4). This suggests that our EDEF stems from the dense plasma (reservoir) at the more eastward/equatorward side. Around 04:08 UT/19.0 LT (Fig. 9c) the DMSP F13 pass was located further to the west, and no plasma density peak was found. Combining Fig. 9a–c implies that (1) a SED was actively developing (possibly westward/poleward by a SAPS) near 273°E GLON around 00:44 UT/19.0 LT (Fig. 9a), (2) at 02:26 UT/19.0 LT (Fig. 9b) it had reached 248°E GLON, and (3) stayed around the GLON sector because at 04:08 UT/19.0 LT (Fig. 9c) it had not reached 221°E GLON. At 04:16 UT/21.3 LT (Fig. 9d) TOPEX passed the region at around 254°E GLON, which is slightly southeastward of the DMSP F13 pass around 02:26 UT (Fig. 9b). TOPEX TEC also exhibits a peak between 45° and 50°S GLAT. As expected this latitudinal profile is wider/smoother than the in situ observations of Fig. 9b. TOPEX records values up to 70 TECU. This is about 40 TECU more than the peak vertical TEC value obtained by CHAMP (see Fig. 6a). This means about 40% of the electron content was above 400 km altitude in the EDEF. DMSP F15 observed a conspicuous plasma density enhancement near 05:07 UT/21.9 LT and 47°S GLAT/252°E GLON (Fig. 9e):

latitudinal width $\sim 2^\circ$ GLAT. The cross-track plasma drift around the density peak was 190 m/s. On the next orbit near 06:49 UT/21.9 LT/226°E GLON DMSP F15 was shifted to the west by about 26°. No conspicuous plasma density enhancement was observed (Fig. 9f): only a marginal enhancement (marked as open circles in Fig. 9i) near 46°S GLAT. The cross-track plasma drift was 150 m/s around the density peak. About 2 h later, around 08:46 UT/0.9 LT, CHAMP observed the EDEF around 48°S GLAT and 242°E GLON (Figs. 2, 5 and 6). It implies that the well-developed SED as observed by DMSP satellites had slowly moved to 242°E GLON by this time and appeared as the EDEF. Around 10:46 UT/2.7 LT (Fig. 4), about 2 h after the CHAMP observations, TIMED/GUVI observed a zonally elongated thin arc between 225°E and 240°E GLON, where CHAMP had observed the EDEF signature. Near 12:28 UT/3.9 LT GRACE observed a weak enhancement of plasma density at 48°S GLAT and 231°E GLON (Fig. 9g), which is reasonably well collocated with the airglow enhancement observed by TIMED/GUVI. The electron densities reported by GRACE are horizontal averages over a meridional distance of about 220 km. This is four times more than the width of the EDEF. Therefore, the amplitude of the density feature appears much reduced. In Fig. 6b is shown the STEC along the ray path from GRACE up to the GPS satellite 03 (PRN-03). The maximum

STEC gradient is 3.1 TECU/degree, which is close to the average post-midnight VTEC gradient during disturbed periods as reported by Vo and Foster (2001). Note that the elevation angle is only 45° in this case. As well as the low data rate of 0.1 Hz, the low elevation angle may have smoothed out the actual gradient, and the actual VTEC gradient may be larger than the observed value (3.1 TECU/degree). About 1.5 h later (13:54 UT/5.8 LT) DMSP F13 passed 238°E GLON and still encountered a small density enhancement at 47°S GLAT (Fig. 9h). In Fig. 9i all the density peaks from DMSP observations are located equatorward of the EDEF as observed by TIMED/GUVI, which seems to result from the large altitude difference between the TIMED/GUVI image (possibly around 350 km) and the DMSP satellites (840 km). The location of the density enhancement corresponds to 40°S MLAT, and the inclination angle of the magnetic field is about 60°. If we follow the magnetic field line, the altitude difference of 500 km ($\approx 840 - 350$ km) will result in horizontal displacement of about 300 km to the southwest. It can explain the position difference of density peaks as observed by DMSP and TIMED/GUVI.

As mentioned in Section 1, a SED generally drifts sunward (Foster et al., 2004). This concept does not fully explain our EDEF observations within a limited GLON range over an extended period (02:26–13:54 UT) by DMSP F13/F15, CHAMP, TIMED/GUVI, and GRACE. It seems that westward drift speed of the EDEF was rather low. Over the 10 h the EDEF has moved westward by about 20° in GLON. This corresponds to an average drift velocity of ~ 40 m/s.

Based on the above-mentioned facts our multi-satellite observations support the following scenario. (1) a SAPS generated a SED in the post-sunset sector near 00:44 UT/19.0 LT/273°E (Fig. 9a). At this time, end of the storm expansion phase (Fig. 1), the active SAPS occurred at rather low latitudes and overlapped well with the poleward expanded equatorial ionization anomaly, a suitable condition for forming a SED. (2) Subsequently, the storm went into a recovery phase, which caused a poleward retreat of the SAPS and a disconnection from the SED between 40°S and 35°S MLAT. (3) A narrow, zonally extended EDEF is left standing at mid-latitudes in the co-rotating F region plasma. Repeated detections by multiple satellites within a limited range of GLON confirmed the stationarity of the structure over at least 10 h. Only a slow westward drift of some 40 m/s is deduced on average. (4) A nearly co-rotating drainage plume in the plasmasphere (i.e. a plume losing contact with the enhanced convection at higher L -shell) has been reported previously (e.g. Spasojević et al., 2003). As drainage plumes are conjugate to SEDs (Foster et al., 2002), the existence of a co-rotating drainage plume indirectly supports our suggestion.

4.4. Ramifications of the post-midnight EDEF

Goi et al. (2009) reported that the occurrence of mid-latitude TEC enhancements, as observed by 1D TEC measurements onboard low-altitude satellites, maximizes at 14–17 LT and 03–05 LT. The enhancements generally span several degrees of GLAT. The authors speculated that different mechanisms work for the dayside and dawnside events. Goi and Saito (2010) attributed the daytime enhancements to SED, and speculated that the dawnside source is photo-ionization associated with midnight sun (white night). As mentioned above, the TEC gradient across our EDEF amounts to about 17 TECU/degree GLAT, so that the TEC difference between the peak and the background is approximately 16 TECU. This amount of TEC change is comparable to those found in the statistical study of Goi et al. (2009). We suggest that a part of their dawnside events can be fossils of pre-midnight SEDs, as reported here.

Recently, Kwon et al. (2012) reported that the energy loss of Pi2 magnetic pulsations (period=40–150 s) is larger on the duskside than on the dawnside (see their Figure 17). The enhanced loss at dusk was attributed to the more complicated plasmaspheric shape, which originates from the plasmaspheric drainage plumes. A SED is conjugate to plasmaspheric plumes (Foster et al., 2002), and our EDEF may also be conjugate to post-midnight plumes reported by Spasojević et al. (2003). In that case the Pi2 energy can be lost significantly even in the post-midnight sector. This may be an interesting topic for a future study.

4.5. Pressure balance across the EDEF boundaries

Let us discuss the pressure balance across the EDEF. The plasma pressure variation across low-latitude plasma density irregularities (such as equatorial plasma bubbles) is in many cases counter-balanced by the magnetic pressure variation, which originates from the pressure gradient currents (diamagnetic effect) (Lühr et al., 2003; Stolle et al., 2006; Park et al., 2008). Here, we calculate the plasma and magnetic pressures across the EDEF in Fig. 2, and check the balance between them. See Section 6 of Park et al. (2010) for details of the calculation. Let us take a nighttime temperature of 1100 K for electrons (based on Fig. 2d), and assume 800 K for the ions. The total (electron+ion) plasma pressure increase from the ambient to the EDEF peak is then ~ 59 nPa. The corresponding decrease of magnetic pressure, calculated from the B-field change of 2.3 nT (Fig. 3c) at an ambient B-field strength of 36 μ T (observed by CHAMP), amounts to -66 nPa. The magnetic pressure gradient compensates well the plasma pressure gradient. This contribution of magnetic pressure helps to keep our confined EDEF stable over more than 10 h.

4.6. Generator of FACs

Besides the diamagnetic effect, we observe also signatures of FACs. The question to be answered is, whether the EDEF acts as a generator or a load in the circuit. If CHAMP had an electric field instrument, we could have answered the question clearly. We may, however, come up with suggestions derived from indirect observations. According to Fig. 2b the zonal wind is practically zero at the location of the EDEF. From our multiple spacecraft observations, we deduced a mean westward drift of ~ 40 m/s for the EDEF. Let us use this velocity as an estimate of the $E \times B$ drift speed of the ambient plasma. With the ambient magnetic field of 36 μ T, westward drift of ~ 40 m/s results in an electric field of $E \sim 1.4$ mV/m pointing southward (poleward). Such a polarity makes the EDEF a FAC generator. For a plausibility check, we calculate the integrated FAC sheet current density, $J = \Delta B_{zonal} / \mu_0 \sim 1.2$ mA/m, where ΔB_{zonal} is the maximum change of B_{zonal} across the EDEF (Fig. 3b). We compare it with the estimated electric field and obtained for the conductance of the conjugate ionosphere, where the circuit closes, a value of $\Sigma \sim 1$ S. This is comparable to the ‘pre-midnight’ sub-auroral Pedersen conductance during storm-time as estimated by Mishin et al. (2003). As the conductivity is expected to be lower past midnight, where our CHAMP observations were made, the estimated value of 1 S can be considered larger than usual storm-time values. Future missions providing precise E and B measurements should be used for studying the electrodynamics of SEDs in more details.

5. Summary

On 30th October 2003, during an intermittent recovery phase of the well-known Halloween storm, CHAMP and TIMED observed

an unusual electron density enhancement fossil (EDEF) past midnight. The EDEF was (1) latitudinally narrow ($\sim 0.5^\circ$ GLAT), (2) zonally elongated ($> 10^\circ$ GLON), and (3) vertically elongated (over several hundreds of kilometers, nearly field-aligned). Magnetic field deflections are primarily confined to the zonal component, which is consistent with a zonally elongated shape of the EDEF and associated FAC sheets. The average direction of FACs is upward (downward) at the equatorward (poleward) edge. The EDEF seems to act as a dynamo generating FACs that is dissipated in the conjugate ionosphere/thermosphere.

At the end of the storm expansion phase a SAPS generated a SED in the post-sunset (19.0 LT) sector. Due to the rapid poleward retreat of the SAPS during the recovery phase the SED turns into an EDEF. This density irregularity at mid-latitude (50° S GLAT) is practically stationary. It persisted and co-rotated past the 3.9 LT sector (remnants are even observed at 5.8 LT). Never before such a long life-time of a SED has been reported. The compensation of plasma pressure variations by the magnetic pressure seems to provide the stability of the EDEF structure for more than 10 h.

It is notable that the plasma irregularity, whose 1D latitudinal profile resembles that of low-latitude plasma blobs (i.e. plasma density enhancements confined within a few degrees of latitude (e.g. see Figures in Park et al., 2008; Kil et al., 2011)), can have the form of a zonally elongated band. EDEFs might also be part of the dawnside mid-latitude TEC enhancements as given in the statistics by Goi et al. (2009).

This is the first dedicated study of a post-midnight fossil of a SED, and the first report on its magnetic signatures. Most of previous works have detected SED by ground-based GPS receivers or radars, so that the results are restricted to the regions above landmasses. We have presented the first 3D image of a SED in the middle of the Pacific Ocean, and proved the suitability of satellite-based remote sensing and in situ measurement techniques to investigate the 3D SED structures outside landmasses. However, more multi-instrument, multi-point observations with high temporal/spatial resolution are needed to complete our understanding. The upcoming *Swarm* mission of the European Space Agency, a constellation of three CHAMP-like satellites, may contribute a lot to the clarification of SED generation/evolution processes.

Acknowledgments

The authors thank Y. Goi for providing her conference presentation material and B. Fejer for valuable comments. We are grateful to the National Oceanic and Atmospheric Administration (NOAA) for providing the POES data, to M. Hairston, the Center for Space Sciences at the University of Texas at Dallas, and the US Air Force for providing the DMSP thermal plasma data. The DMSP particle detectors were designed by Dave Hardy of AFRL, and data obtained from JHU/APL. The OMNI data were obtained from the GSFC/SPDF OMNIWeb interface at <http://omniweb.gsfc.nasa.gov>. The GUVI data used here are provided through support from the NASA MO and DA program. The GUVI instrument was designed and built by The Aerospace Corporation and The Johns Hopkins University. The Principal Investigator is Dr. Andrew B. Christensen and the Chief Scientist and co-PI is Dr. Larry J. Paxton. The CHAMP mission is sponsored by the Space Agency of the German Aerospace Center (DLR) through funds of the Federal Ministry of Economics and Technology, following a decision of the German Federal Parliament (grant code 50EE0944). The data retrieval and operation of the CHAMP satellite by the German Space Operations Center (GSOC) is acknowledged. H. Kil acknowledges support from the National Science Foundation National Space Weather Program (AGS-1024886). G. Jee acknowledges support from project PE12010 funded by the Korea Polar Research Institute.

References

- Datta-Barua, S., Bust, G.S., Crowley, G., 2011. Deducing storm time F region ionospheric dynamics from 3-D time-varying imaging. *Journal of Geophysical Research* 116, A05324. <http://dx.doi.org/10.1029/2010JA016304>.
- Drayton, R.A., Koustov, A.V., Hairston, M.R., Villain, J.-P., 2005. Comparison of DMSP cross-track ion drifts and SuperDARN line-of-sight velocities. *Annals of Geophysics* 23, 2479–2486. <http://dx.doi.org/10.5194/angeo-23-2479-2005>.
- Foster, J.C., 1993. Storm time plasma transport at middle and high latitudes. *Journal of Geophysical Research* 98 (A2), 1675–1689.
- Foster, J.C., Vo, H.B., 2002. Average characteristics and activity dependence of the sub-auroral polarization stream. *Journal of Geophysical Research* 107 (A12), 1475. <http://dx.doi.org/10.1029/2002JA009409>.
- Foster, J.C., Erickson, P.J., Coster, A.J., Goldstein, J., Rich, F.J., 2002. Ionospheric signatures of plasmaspheric tails. *Geophysical Research Letters* 29 (13), 1623. <http://dx.doi.org/10.1029/2002GL015067>.
- Foster, J.C., Coster, A.J., Erickson, P.J., Rich, F.J., Sandel, B.R., 2004. Stormtime observations of the flux of plasmaspheric ions to the dayside cusp/magnetopause. *Geophysical Research Letters* 31. <http://dx.doi.org/10.1029/2004GL020082>.
- Foster, J.C., Rideout, W., Sandel, B., Forrester, W.T., Rich, F.J., 2007. On the relationship of SAPS to storm-enhanced density. *Journal of Atmospheric and Solar-Terrestrial Physics* 69, 303–313.
- Foster, J.C., Rideout, W., 2007. Storm enhanced density: magnetic conjugacy effects. *Annals of Geophysics* 25, 1791–1799.
- Goi, Y., Saito, A., Nishioka, M., 2009. Vertical structures of the TEC enhancement at mid-latitudes in the morning and the daytime sectors. *American Geophysical Union, Fall Meeting 2009*, abstract SA33A-1442.
- Goi, Y., Saito, A., 2010. Study of characteristic appearance of TEC enhancement at mid-latitude using TEC data. In: 38th COSPAR Scientific Assembly, July 2010, p. 3.
- Goldstein, J., Sandel, B.R., Hairston, M.R., Reiff, P.H., 2003. Control of plasmaspheric dynamics by both convection and subauroral polarization stream. *Geophysical Research Letters* 30, 2243. <http://dx.doi.org/10.1029/2003GL018390>.
- Greenspan, M.E., Rasmussen, C.E., Burke, W.J., Abdu, M.A., 1991. Equatorial density depletions observed at 840 km during the great magnetic storm of March 1989. *Journal of Geophysical Research* 96 (A8), 13,931–13,942. <http://dx.doi.org/10.1029/91JA01264>.
- Heise, S., Jakowski, N., Wehrenpfennig, A., 2002. Imaging the ionosphere/plasmasphere based on GPS data obtained onboard CHAMP. *EGS XXVII General Assembly, Nice, France, April 2002*.
- Immel, T.J., Mende, S.B., Frey, H.U., Peticolas, L.M., Carlson, C.W., Gérard, J.-C., Hubert, B., Fuselier, S.A., Burch, J.L., 2002. Precipitation of auroral protons in detached arcs. *Geophysical Research Letters* 29 (11), 1519. <http://dx.doi.org/10.1029/2001GL013847>.
- Jakowski, N., Jungstand, A., Lois, L., Lazo, B., 1991. Night-time enhancements of the F2-layer ionization over Havana, Cuba. *Journal of Atmospheric and Terrestrial Physics* 53, 1131–1138.
- Jakowski, N., Heise, S., Wehrenpfennig, A., Schlüter, S., Reimer, R., 2002. GPS/GLONASS-based TEC measurements as a contributor for space weather forecast. *Journal of Atmospheric and Solar-Terrestrial Physics* 64, 729–735.
- Kasahara, Y., Hosoda, T., Mukai, T., Watanabe, S., Kimura, I., Kojima, H., Niitsu, R., 2001. ELF/VLF waves correlated with transversely accelerated ions in the auroral region observed by Akebono. *Journal of Geophysical Research* 106, 21123–21136. <http://dx.doi.org/10.1029/2000JA000318>.
- Kelley, M.C., Vlasov, M.N., Foster, J.C., Coster, A.J., 2004. A quantitative explanation for the phenomenon known as storm-enhanced density. *Geophysical Research Letters* 31, L19809. <http://dx.doi.org/10.1029/2004GL020875>.
- Keyser, H.L., Green, B.S., della-Rose, D.J., Sojka, J.J., Erickson, P.J., Hairston, M.R., Rich, F.J., 2003. Comparison of DMSP SSIEs density and temperature measurements with ground-based incoherent scatter radar data. *American Geophysical Union, Fall Meeting 2003*, abstract SA21B-0085.
- Kil, H., Su, S.-Y., Paxton, L.J., Wolven, B.C., Zhang, Y., Morrison, D., Yeh, H.C., 2004. Coincident equatorial bubble detection by TIMED/GUVI and ROCSAT-1. *Geophysical Research Letters* 31, L03809. <http://dx.doi.org/10.1029/2003GL018696>.
- Kil, H., Choi, H.S., Heelis, R.A., Paxton, L.J., Coley, W.R., Miller, E.S., 2011. Onset conditions of bubbles and blobs: a case study on 2 March 2009. *Geophysical Research Letters* 38, L06101. <http://dx.doi.org/10.1029/2011GL046885>.
- Kwon, H.-J., et al., 2012. Local time-dependent Pi2 frequencies confirmed by simultaneous observations from THEMIS probes in the inner magnetosphere and at low-latitude ground stations. *Journal of Geophysical Research* 117, A01206. <http://dx.doi.org/10.1029/2011JA016815>.
- Lee, J.J., Min, K.W., Kim, V.P., Hegai, V.V., Oyama, K.-I., Rich, F.J., Kim, J., 2002. Large density depletions in the nighttime upper ionosphere during the magnetic storm of July 15, 2000. *Geophysical Research Letters* 29 (3), 1032. <http://dx.doi.org/10.1029/2001GL013991>.
- Liu, C., Horwitz, J.L., Richards, P.G., 1995. Effects of frictional ion heating and soft-electron precipitation on high-latitude F-region upflows. *Geophysical Research Letters* 22 (20), 2713–2716. <http://dx.doi.org/10.1029/95GL02551>.
- Liu, H., Lühr, H., Henize, V., Köhler, W., 2005. Global distribution of the thermospheric total mass density derived from CHAMP. *Journal of Geophysical Research* 110, A04301. <http://dx.doi.org/10.1029/2004JA010741>.
- Liu, H., Lühr, H., Watanabe, S., Köhler, W., Henize, G., Visser, P., 2006. Zonal winds in the equatorial upper thermosphere: decomposing the solar flux, geomagnetic activity, and seasonal dependencies. *Journal of Geophysical Research* 111, A07307. <http://dx.doi.org/10.1029/2005JA011415>.

- Liu, H., Stolle, C., Watanabe, S., 2007. Evaluation of the IRI model using CHAMP observations in polar and equatorial regions. *Advances in Space Research* 39, 904–909.
- Lühr, H., Rother, M., Maus, S., Mai, W., Cooke, D., 2003. The diamagnetic effect of the equatorial Appleton anomaly: its characteristics and impact on geomagnetic field modeling. *Geophysical Research Letters* 30, 1906. <http://dx.doi.org/10.1029/2003GL017407>.
- Lühr, H., Rother, M., Köhler, W., Ritter, P., Grunwaldt, L., 2004. Thermospheric upwelling in the cusp region: evidence from CHAMP observations. *Geophysical Research Letters* 31, L06805. <http://dx.doi.org/10.1029/2003GL019314>.
- Lühr, H., Xiong, C., 2010. IRI-2007 model overestimates electron density during the 23/24 solar minimum. *Geophysical Research Letters* 37, L23101. <http://dx.doi.org/10.1029/2010GL045430>.
- McNamara, L.F., Cooke, D.L., Valladares, C.E., Reinisch, B.W., 2007. Comparison of CHAMP and Digisonde plasma frequencies at Jicamarca, Peru. *Radio Science* 42, RS2005. <http://dx.doi.org/10.1029/2006RS003491>.
- Mishin, E.V., Burke, W.J., Huang, C.Y., Rich, F.J., 2003. Electromagnetic wave structures within subauroral polarization streams. *Journal of Geophysical Research* 108 (A8), 1309. <http://dx.doi.org/10.1029/2002JA009793>.
- Park, J., Stolle, C., Lühr, H., Rother, M., Su, S.-Y., Min, K.W., Lee, J.-J., 2008. Magnetic signatures and conjugate features of low-latitude plasma blobs as observed by the CHAMP satellite. *Journal of Geophysical Research* 113, A09313. <http://dx.doi.org/10.1029/2008JA013211>.
- Park, J., Lühr, H., Min, K.W., 2010. Neutral density depletions associated with equatorial plasma bubbles as observed by the CHAMP satellite. *Journal of Atmospheric and Solar-Terrestrial Physics* 72, 157–163.
- Pokhotelov, D., Mitchell, C.N., Spencer, P.S.J., Hairston, M.R., Heelis, R.A., 2008. Ionospheric storm time dynamics as seen by GPS tomography and in situ spacecraft observations. *Journal of Geophysical Research* 113, A00A16. <http://dx.doi.org/10.1029/2008JA013109>.
- Pryse, S.E., Wood, A.G., Middleton, H.R., McCrea, I.W., Lester, M., 2006. Reconfiguration of polar-cap plasma in the magnetic midnight sector. *Annals of Geophysics* 24, 2201–2208. <http://dx.doi.org/10.5194/angeo-24-2201-2006>.
- Rother, M., Schlegel, K., Lühr, H., Cooke, D., 2010. Validation of CHAMP electron temperature measurements by incoherent scatter radar data. *Radio Science* 45, RS6020. <http://dx.doi.org/10.1029/2010RS004445>.
- Sakaguchi, K., Shiokawa, K., Ieda, A., Miyoshi, Y., Otsuka, Y., Ogawa, T., Connors, M., Donovan, E.F., Rich, F.J., 2007. Simultaneous ground and satellite observations of an isolated proton arc at subauroral latitudes. *Journal of Geophysical Research* 112, A04202. <http://dx.doi.org/10.1029/2006JA012135>.
- Schunk, R.W., 2000. Theoretical developments on the causes of ionospheric outflow. *Journal of Atmospheric and Solar-Terrestrial Physics* 62 (6), 399. [http://dx.doi.org/10.1016/S1364-6826\(00\)00017-1](http://dx.doi.org/10.1016/S1364-6826(00)00017-1).
- Spasojević, M., Goldstein, J., Carpenter, D.L., Inan, U.S., Sandel, B.R., 2003. Global response of the plasmasphere to a geomagnetic disturbance. *Journal of Geophysical Research* 108, 1340. <http://dx.doi.org/10.1029/2003JA009987>.
- Stolle, C., Lühr, H., Rother, M., Balasis, G., 2006. Magnetic signatures of equatorial spread F, as observed by the CHAMP satellite. *Journal of Geophysical Research* 111, A02304. <http://dx.doi.org/10.1029/2005JA011184>.
- Tsurutani, B., et al., 2004. Global dayside ionospheric uplift and enhancement associated with interplanetary electric fields. *Journal of Geophysical Research* 109, A08302. <http://dx.doi.org/10.1029/2003JA010342>.
- Vlasov, M., Kelley, M.C., Kil, H., 2003. Analysis of ground-based and satellite observations of F-region behavior during the great magnetic storm of July 15, 2000. *Journal of Atmospheric and Solar-Terrestrial Physics* 65, 1223–1234.
- Vo, H.B., Foster, J.C., 2001. A quantitative study of ionospheric density gradients at midlatitudes. *Journal of Geophysical Research* 106 (A10), 21,555–21,563.
- Wang, H., Lühr, H., Ma, S.Y., Weygand, J., Skoug, R.M., Yin, F., 2006. Field-aligned currents observed by CHAMP during the intense 2003 geomagnetic storm events. *Annals of Geophysics* 24, 311–324.
- Wang, H., Lühr, H., Häusler, K., Ritter, P., 2011a. Effect of subauroral polarization streams on the thermosphere: a statistical study. *Journal of Geophysical Research* 116, A03312. <http://dx.doi.org/10.1029/2010JA016236>.
- Wang, H., Lühr, H., 2011b. The efficiency of mechanisms driving subauroral polarization streams (SAPS). *Annals of Geophysics* 29, 1277–1286. <http://dx.doi.org/10.5194/angeo-29-1277-2011>.
- Wen, D., Yuan, Y., Ou, J., Zhang, K., Liu, K., 2008. A hybrid reconstruction algorithm for 3-D ionospheric tomography. *IEEE Transactions on Geoscience and Remote Sensing* 46 (6), 1733.
- Xiong, C., Park, J., Lühr, H., Stolle, C., Ma, S.Y., 2010. Comparing plasma bubble occurrence rates at CHAMP and GRACE altitudes during high and low solar activity. *Annals of Geophysics* 28, 1647–1658. <http://dx.doi.org/10.5194/angeo-28-1647-2010>.
- Yizengaw, E., Moldwin, M.B., Dyson, P.L., Immel, T.J., 2005. Southern Hemisphere ionosphere and plasmasphere response to the interplanetary shock event of 29–31 October 2003. *Journal of Geophysical Research* 110, A09S30. <http://dx.doi.org/10.1029/2004JA010920>.
- Yizengaw, E., Moldwin, M.B., Galvan, D.A., 2006. Ionospheric signatures of a plasmaspheric plume over Europe. *Geophysical Research Letters* 33, L17103. <http://dx.doi.org/10.1029/2006GL026597>.
- Yizengaw, E., Dewar, J., MacNeil, J., Moldwin, M.B., Galvan, D., Sanny, J., Berube, D., Sandel, B., 2008. The occurrence of ionospheric signatures of plasmaspheric plumes over different longitudinal sectors. *Journal of Geophysical Research* 113, A08318. <http://dx.doi.org/10.1029/2007JA012925>.